Interface elasticity in nanostructured silicon

Pier Luca Palla,* Stefano Giordano,† and Luciano Colombo‡
Department of Physics, University of Cagliari, Monserrato, I-09042 Cagliari, Italy and Sardinian Laboratory for Computational Materials Science SLACS (INFM-CNR), Cittadella Universitaria, Monserrato, I-09042 Cagliari, Italy
(Received 27 February 2009; revised manuscript received 23 July 2009; published 12 August 2009)

We investigate through atomistic simulations the mechanical behavior of a c-Si nanowire embedded in an elastically different c-Si. The results are compared with the continuum predictions based on the elasticity theory. The observed deviations between the two approaches are due to the presence of the disordered interface in the atom-resolved system which, for small wires, induces sizable prestrain into the sample, also in absence of any external loads. Finally, we develop a continuum model fully exploiting such interface effects provided by the atomistic simulations.

DOI: 10.1103/PhysRevB.80.054105 PACS number(s): 68.35.−p

I. INTRODUCTION

The mechanical behavior of nanostructured materials is strongly affected by interface features, occurring at the boundary between phases characterized by different elastic constitutive equations or crystalline structures.[1,2] In particular, the embedding of a given nanoinclusion in a hosting homogeneous matrix is deeply influenced by the lattice mismatch, which ultimately governs the effective elastic properties of the heterogeneous system. In fact, both the inclusion and the matrix accomplish an elastic relaxation to accommodate this mismatch and, therefore, they admit a state of deformation even if no external load is applied. We will refer to such a complex system as a prestressed (or, equivalently, prestrained) composite.

A typical example of prestressed system is represented by semiconductor quantum dots or quantum wires, embedded in a matrix with different lattice parameter.[3,4] Several works have been addressed to the calculation of the strain state in buried quantum dots.[5–7] Both quantitative and qualitative knowledge of stress and strain distributions are essential for characterizing and tailoring their optoelectronic properties,[8,9] as well as for understanding their self-organization.[10] Typically, the state of deformation is estimated using continuum elasticity and, then, used as input for an electronic structure calculation.[11] However, while continuum elasticity is inherently scale independent, the elastic relaxation of a nanostructure does depend on the actual length scale at which the heterogeneity shows up. In other words, at the nanoscale surface effects become important due to the increasing surface-to-volume ratio and induce a size dependency in the overall elastic behavior.[12,13]

The experimental evidence of this scale effect phenomenon has been addressed in a wide range of contexts.[14] For example, the effects of the reduced size on the elastic properties of nanowires have been measured by atomic force microscopy (AFM) and the increase of the effective elastic modulus for the smaller diameters has been attributed to surface effects.[15] Similar results have been obtained through a nanometer-scale bending test on a c-Si beam, using again AFM methodologies.[16] More recently, the size-dependent effective Young modulus of silicon nanocantilevers have been measured by using electrostatic pull-in instability, within the framework of the nanoelectromechanical systems (NEMS).[17]

In this work we use a combination of atomistic and continuum methods to describe the elastic behavior of a silicon nanowire embedded in a silicon homogeneous matrix with different crystal orientation. This structure represents a good model for real systems of large technological interest.[18–20] Moreover, it also represents a conceptually relevant case where the atomic structure leads to deviations from the standard continuum picture. We describe how the presence of a disordered interface affects the elastic fields and generates a size-dependent prestrain in both the nanowire and the surrounding matrix. In addition, by looking at the mechanical response of this model system to a remote load, we show how the prestrain induces a strong localization of the elastic fields nearby the inclusion. The atomistic simulations are developed to obtain a fully resolved picture of the structural complexity of the disordered interface. On the other hand, a continuum model is here developed, fully exploiting the observed atomistic phenomena. This atomically informed continuum model does include the size-dependent effects described above.

The present paper is structured as follows: in Sec. II we describe the atomistic model of the inclusion, in Sec. III its continuum counterpart is developed and, finally, in Sec. IV we discuss the elastic behavior under external loading by means of both atomistic simulations and continuum models.

II. ATOMISTIC MODEL

We consider a crystalline silicon (c-Si) homogeneous matrix and we fix the x axis along the (100) crystallographic direction of the diamond lattice (see Fig. 1). The lattice parameter is set to the equilibrium value so as to obtain a stress-free configuration. A cylindrical portion of the matrix of radius R is then rotated by an angle ϑ around the z axis (see Fig. 1). Because of the cubic symmetry of the diamond lattice, the rotated cylinder behaves, upon loading along the y axis, as an inclusion with a different elastic response than the hosting matrix. In addition, the elastic mismatch between the inclusion and the matrix depends on the angle of rotation and vanishes for $\vartheta = k\pi/2$ (k=integer). In most of our simulations we fixed $\vartheta = \pi/4$ since this angle supplies the largest

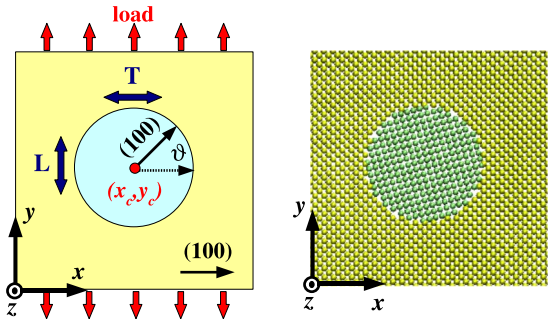

FIG. 1. (Color online) A c-Si inclusion of radius R embedded in a Si matrix. General scheme of the system geometry (left panel) and snapshot of an atomistic sample (right panel). The elastic mismatch between the inclusion and the matrix is obtained through a rotation by an angle ϑ of the inclusion. We also show the direction of the applied deformation (y axis) and those of the longitudinal (l) and of the transverse (t) displacements.

difference in the elastic response between the inclusion and the matrix (see Sec. IV for details).

The interaction among silicon atoms is described by the Tersoff potential.[21] The simulation cell is a thin slab orthogonal to the z axis; periodic boundary conditions are applied so as to obtain an infinite cylindrical inclusion. To minimizing the interaction between the periodic images, the width of the slab is ten times larger than the diameter of the inclusion, both in the x and in the y directions. As for the mechanical behavior, this structure is described by two-dimensional elastic fields (plain strain conditions). It means that all the relevant quantities are functions only of the x and y coordinates.

By generating the input structure as above, we have arranged several samples with $2\ \text{nm} < R < 20\ \text{nm}$. The largest simulated system contains as many as 1.3×10^7 atoms and the corresponding length of the simulation cell along x and y is as large as 400 nm.

The initial configurations have been relaxed through damped dynamics in order to allow for chemical bonding at the interface between the inclusion and the matrix. The convergence criterion is set so to have interatomic forces in the final configuration not larger than 10^{-5} eV/Å. After this relaxation, we have computed the atomic displacement field $\vec{u}^0(x,y)$ and we have found that the disordered interface generates a uniform hydrostatic compression within the inclusion. Therefore, the present atomistic model correctly predicts that even in absence of any external load, the inclusions exhibit a state of uniform internal prestrain. In Fig. 2 we show the variation of such a prestrain $\varepsilon^0 = \partial u_x^0/\partial x = \partial u_y^0/\partial y$ as function of the radius R. In order to obtain ε^0 for each sample, we have fit the $u_x^0(x,y)$ and $u_y^0(x,y)$ surfaces inside the inclusion guessing a linear dependence on x and y. In order to test the linear hypothesis, i.e., the uniformity of the internal strain field, we have used several fitting domains obtaining a constant trend.

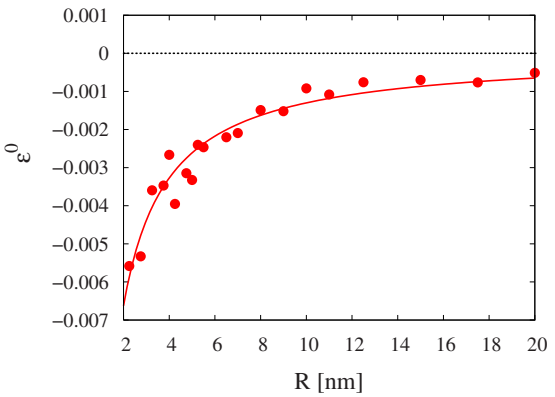

FIG. 2. (Color online) Internal prestrain ε^0 within the nanowire as a function of the inclusion radius R. We report the atomistic result (full symbols) and the continuum theory prediction (solid line).

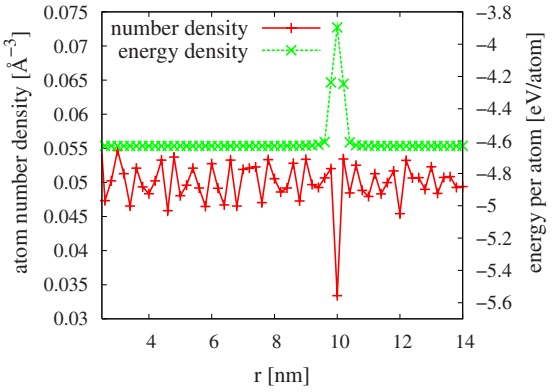

FIG. 3. (Color online) Energy per atom and atom number density as a function of the distance r from the center of the inclusion of radius R. The data correspond to a sample with $R = 10.0$ nm. For $r \simeq R$ the local number density is much smaller than elsewhere while the energy, as expected, is higher.

In Fig. 2 we note that the prestrain ε^0 (in absolute value) reduces with increasing R. This effect can be explained as follows. In Fig. 3 we report the atom number density and the energy per atom as a function of the distance r from the center of the inclusion; data are obtained from the sample with $R = 10$ nm. We note that the atom number density at a distance $r = R$, corresponding to the position of the interface, is lower than its value in the surrounding crystalline bulk. The interface region behaves as a coating of constant thickness d inserted between the matrix and the inclusion. Therefore, the volume available for the inclusion is reduced with respect to the initial configuration by a factor $(\frac{R-d}{R})^2$. When R increases this volume variation and the resulting prestrain tend to zero. We remark that, in principle, the thickness of the disordered interface could depend on the value of the angle ϑ defined in Fig. 1. Nevertheless, in our calculations such a thickness was found to be pretty constant, as discussed below (see Sec. III). Further investigations about the disordered structure at an interface can be found elsewhere.[22,23]

III. CONTINUUM MODEL

In the previous section we proved that the prestrain within the inclusion does depend on its size because of interface effects. Here this result is considered as a guideline for the

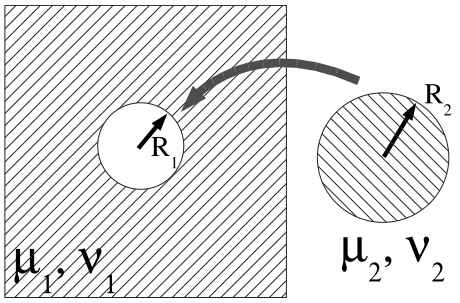

FIG. 4. Scheme of the continuum theory model of a prestrained inclusion. Its radius R_2 is bigger then the radius R_1 of the hole in the host matrix (both defined in the reference undisturbed configuration). The elastic properties of the two media are represented by the shear modulus μ_α and by the Poisson ratio ν_α, where $\alpha=1,2$.

development of a continuum model reproducing the elastic features of the atom-resolved system. We consider the configuration represented in Fig. 4, where a cylinder of radius R_2 is forced to fit a similarly shaped void with radius $R_1<R_2$. We also assume that both the hosting matrix and the cylinder are made of isotropic materials described by the elastic moduli (μ_1,ν_1) and (μ_2,ν_2), respectively (μ is the shear modulus and ν is the Poisson ratio).

When $R_2>R_1$ a uniform compression inside the cylinder is generated, as well as a radially decreasing compression in the external region. For the following purposes, we are also interested in the determination of the elastic fields when an arbitrary load is remotely applied. This model must lead the classical Eshelby results when $R_2=R_1$, i.e., when prestrain and prestress are zero.[24,25]

The elastic field has been obtained through the complex potentials methods due to Kolossov and Muskhelishvili.[26–28] This robust approach to elasticity was recently adopted to solve several two-dimensional (plane-elasticity) nanomechanics problems.[29,30] In Appendix A we will show the details of this calculation. In order to apply this model to the problem described in Sec. II, we have to set its elastic parameters (i.e., μ_1, ν_1, μ_2, and ν_2) consistently. This implies that we must introduce two different isotropic media, respectively, describing the elastic behavior of the nanowire and of the matrix. If the linear elasticity of the matrix is described by the stiffness tensor $\hat{C}^{(100)}$, then the inclusion is represented (in the same system of reference) by the tensor $\hat{C}^{(100)}$ rotated upon the z axis, namely, $\hat{C}(\vartheta)$ (remember that in our case both the matrix and the inclusion are made of c-Si). On the other hand, the isotropic elastic moduli μ and ν for the two phases depend upon the stiffness tensor components through the following relations:

$$\mu=(C_{11}-C_{12})/2,$$

$$\nu=C_{12}/(C_{11}+C_{12}). \tag{1}$$

Therefore, we set

$$\mu_1=(C_{11}^{(100)}-C_{12}^{(100)})/2,$$

$$\nu_1=C_{12}^{(100)}/(C_{11}^{(100)}+C_{12}^{(100)}) \tag{2}$$

in the matrix and

$$\mu_2=[C_{11}(\vartheta)-C_{12}(\vartheta)]/2,$$

$$\nu_2=C_{12}(\vartheta)/[C_{11}(\vartheta)+C_{12}(\vartheta)], \tag{3}$$

in the inclusion. This approach is fully justified because we have calculated the exact internal strain field for some paradigmatic configurations with the anisotropic Eshelby model[31,32] and we have verified that our isotropic approximation does not affect the results under uniaxial elongations or hydrostatic external loadings.

On the other hand, the formalism for the isotropic case is much lighter than for the anisotropic one,[33] thus providing a more clean picture. Therefore, the choice of an isotropic continuum model derives from the observation that the complex potentials method extended to anisotropic materials[33] is so complicated to nullify all the advantages of a simple model that can be used appreciating the underlying physical meaning.

The results of the atomistic simulations (full symbols in Fig. 2) have been fitted by means of the analytic expression for the prestrain (see Appendix A)

$$\varepsilon^0=\frac{\mu_1(\chi_2-1)(R_1-R_2)}{2\mu_2R_1-\mu_1R_2+R_2\mu_1\chi_2}, \tag{4}$$

where $\chi_2=3-4\nu_2$. The radius difference $\Delta R=R_2-R_1$ has been considered as the fitting parameter. Moreover, in order to draw the comparison with the atomistic simulations we have imposed $(R_1+R_2)/2=R$. Therefore, Eq. (4) is recast in the form

$$\varepsilon^0=-\frac{\mu_1(1-2\nu_2)\Delta R}{\mu_2\left(R-\frac{\Delta R}{2}\right)+\mu_1(1-2\nu_2)\left(R+\frac{\Delta R}{2}\right)}. \tag{5}$$

The fitting procedure provided a value $\Delta R=R_2-R_1=0.6$ Å, and proved that the present continuum model is consistent with atomistic data, as shown in Fig. 2. This important result stands for the fact that the width of the disordered interface region can be considered independent from the curvature of the interface (at least in the present context); rather, it depends only on the crystalline structure of the two materials.

IV. EFFECT OF EXTERNAL LOADING

An uniaxial homogeneous elongation of 1% along the y direction (corresponding to a displacement field $u_x=0$ and $u_y=\varepsilon_{yy}^{\infty}y$, where $\varepsilon_{yy}^{\infty}=0.01$) was applied to the samples described in Sec. II. After the relaxation of the atomistic structure (performed through damped dynamics with the same convergence criterion reported in Sec. II), we have computed both the longitudinal $u_y(x,y)$ and the transverse $u_x(x,y)$ displacement fields inside and outside the embedded inclusion.

As a first step, we checked whether the internal strain could be considered as a uniform field, as predicted by the continuum elasticity.[24] We have found that this prediction is indeed well verified by atomistic simulations, provided that

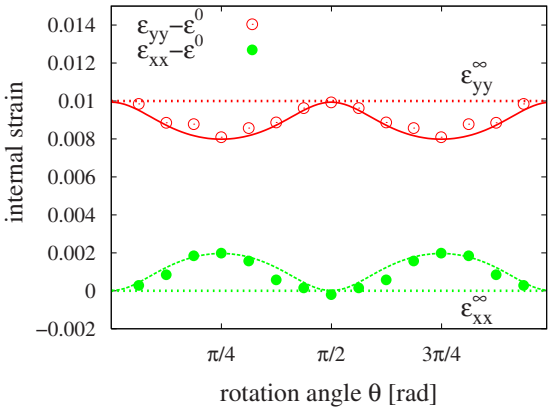

FIG. 5. (Color online) Longitudinal ε_{yy} (empty symbols) and transverse ε_{xx} (full symbols) strain inside the inclusion after the application of the load to the sample with $R=2$ nm. We show the difference between these strain components and the corresponding prestrain (ε^0) as a function of the rotation angle ϑ. We also report the values ($\varepsilon^\infty_{yy}=0.01$ and $\varepsilon^\infty_{xx}=0$) of the strain applied to the overall system (horizontal dotted lines). The solid and the dashed curves represent the continuum theory predictions for the longitudinal and for the transverse field, respectively.

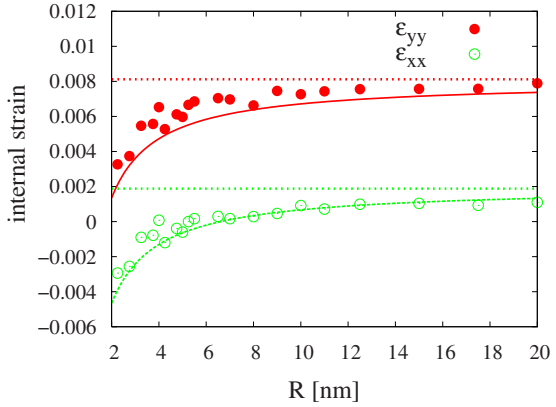

FIG. 6. (Color online) Longitudinal (ε_{yy}) and transverse (ε_{xx}) internal strain components as a function of the radius R of the cylindrical inclusion. Full and dashed lines represent the continuum theory. We also show by dotted lines the corresponding asymptotic values approached when the interface-induced prestrain becomes negligible.

we neglect a narrow disordered coating (about 0.5 nm thick) close to the interface. In order to obtain these estimations we have applied a fitting procedure similar to that used for the prestrain calculation (see Sec. II).

A further analysis has been performed to investigate the dependence of the internal strain upon the elastic mismatch between the inclusion and the matrix described by the rotation angle ϑ as shown in Eqs. (2) and (3). In Fig. 5, we show the differences $\varepsilon_{xx}-\varepsilon^0$ and $\varepsilon_{yy}-\varepsilon^0$ between the resulting internal strain (after the application of the load) and the prestrain as function of ϑ for an inclusion with $R=2$ nm. As expected for a cubic crystal like c-Si, both the longitudinal (empty symbols in Fig. 5) and transverse (full symbols in Fig. 5) strain components are $\pi/2$-periodic. Moreover, the angle $\vartheta=\pi/4$ leads to the largest difference between the internal strain and the applied one. In Fig. 5 we also report the results obtained through the atomically informed continuum model described in Sec. III (full and dashed lines). We note a good agreement between atomistics and continuum and we remark that for $\vartheta=\pi/2$ the inclusion has the same crystallographic orientation of the matrix. Nevertheless, a disordered interface and the corresponding prestrain are present. This is due to the fact that a pure $\pi/2$-rotation does not arrange the atoms consistently with the surrounding crystal [in order to obtain such a correspondence we have to apply a suitable translation along the (111) direction as well]. Interesting enough, we found $\varepsilon_{xx}-\varepsilon^0=\varepsilon^\infty_{xx}$ and $\varepsilon_{yy}-\varepsilon^0=\varepsilon^\infty_{yy}$ for $\vartheta=\pi/2$, where ε^∞_{xx} and ε^∞_{yy} are the components of the remotely applied strain field. In other words, in spite of the complexity of the continuum equations described in Appendix A, the prestrain roughly acts as an additive constant to the applied strain.

In Fig. 6 we report the longitudinal (ε_{yy}) and transverse (ε_{xx}) strain fields inside the inclusion under load versus the inclusion radius R (for $\vartheta=\pi/4$). The results of the continuum theory are obtained by setting the prestrain to the value stated by the fitting procedure of the atomistic data (see Sec. III). For large values of the radius, the effect of the interface-induced prestrain is negligible (see also Fig. 2) and the elastic fields become size independent. Moreover, in the limit of vanishing prestrain (or equivalently for $R\to\infty$, as shown in Fig. 2), the constant values approached by the atomistic data correspond to those predicted by the Eshelby continuum model.[24]

Finally, we have investigated the effect of the inclusion on the surrounding matrix. Also in this case, we have found that the prestrain plays an important role in the determination of the elastic state of deformation of the system. In Fig. 7 we show the longitudinal displacement field across the inclusion ($R=10$ nm). In order to magnify the effects, we report the perturbation $u_y(x_c,y)-\varepsilon^\infty_{yy}y$ to the uniform applied displacement (where x_c is the abscissa of the center of the inclusion).

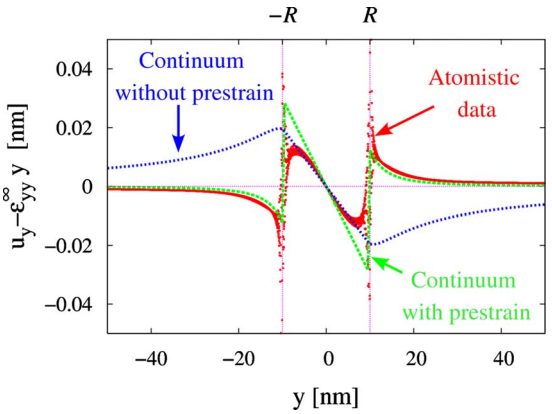

FIG. 7. (Color online) Longitudinal displacement $u_y(x,y)$ showing the behavior of the elastic field across the inclusion ($R=10$ nm). The continuum predictions (blue and green curves) have been obtained by imposing $x=x_c$, where x_c corresponds to the center of the inclusion. The atomistic data (red dots) represent the displacement in the set of atoms having $x\in(x_c-\Delta x,x_c+\Delta x)$ where $\Delta x=1$ nm. In order to better detect the effect of the inclusion, we report the difference, $u_y(x_c,y)-0.01y$, between the longitudinal field and the uniform applied displacement of 1% in the y direction.

We have reported two different predictions obtained through the continuum model described in Sec. III and in Appendix A. Corresponding atomistic data (red dots) are reported as well. The dashed green line represents the effect of the remotely applied load to the prestrained system and it is in good agreement with the atomistic scenario. The dotted blue curve shows the behavior of the system under load when the prestrain is absent. By comparing the two continuum models, we note that the internal fields are quite similar and the difference roughly corresponds to ε^0. On the contrary, the external fields are completely different. In the model including prestrain, the curve in Fig. 7 exhibits a very fast decay to zero. In other words, the prestrain causes a strong localization of the elastic fields around the interface. This effect is associated with a loss of continuity of the displacement field due to the narrow interface region which separates the two bulk zones. It is interesting to observe that our atomically informed continuum model perfectly takes into account both the fast decay and the displacement discontinuity, being in good agreement with the atomistic simulations.

V. CONCLUSIONS

In this paper we have described several atomistic simulations performed to investigate the elastic behavior of a c-Si inclusion embedded in a differently oriented c-Si matrix. In particular, we have described the effects of the presence of a prestrain, which is experimentally observed in many real cases.[8] In addition, we have analyzed the elastic strain field in the system both with and without a remotely applied external loading. Moreover, we have developed an elastic model (framed within continuum mechanics) fully exploiting the main atomic-scale features. We have proved that the generalization of the standard Eshelby theory (with a simple hydrostatic prestrain inside the inclusion) is sufficient to correctly describe the overall elastic behavior of the embedded structure. In this work we have focused on a circular shape of the inclusion: of course, both the analytical model and the computational procedure can be generalized in order to take into account an elliptic shape with arbitrary aspect ratio. In fact, as it is well known, the Eshelby theory is able to consider any elliptic shape in two-dimensional elasticity or any ellipsoidal shape in three-dimension elasticity.[31] Moreover, it is important to remark that our results have been obtained for the crystalline silicon, but they can be transferred to other covalently bonded materials as well and, more generally, to brittle and ceramic systems. As for to the applications, we underline that this investigation can be directly used to analyze the generation of prestrain during the embedding or the self-assembling of nanoparticles, such as quantum dots and quantum wires, in a matrix with different structure and physical properties. In particular, we have discussed the phenomenon of the localization of the elastic fields in the neighborhood of the inclusion, modulated by the actual prestrain.

ACKNOWLEDGMENTS

We acknowledge financial and computational support by MiUR under project PON—"CyberSar" (OR 7) and computational support by CASPUR (Rome, Italy).

APPENDIX A: SOLUTION OF THE CONTINUUM MODEL

In order to solve the model presented in Sec. III, we use the complex variable method for the two-dimensional elasticity.[34] In each homogeneous region of the xy plane the displacement vector field and the stress tensor field can be represented by means of a couple of Kolossov-Muskhelishvili elastic potentials.[26–28] We assume that the elastic state of a given homogeneous region α is exactly described by two holomorphic functions $\phi_\alpha(z)$ and $\psi_\alpha(z)$, where the complex number $z=x+iy$ represents the position on the plane. The Kolossov-Muskhelishvili equations allow for the determination of the elastic fields in each region[28]

$$u_x^\alpha + iu_y^\alpha = \frac{1}{2\mu_\alpha}[\chi_\alpha \phi_\alpha(z) - z\overline{\phi'_\alpha(z)} - \overline{\psi_\alpha(z)}], \tag{A1}$$

$$\sigma_{xx}^\alpha + \sigma_{yy}^\alpha = 2[\phi'_\alpha(z) + \overline{\phi'_\alpha(z)}], \tag{A2}$$

$$\sigma_{yy}^\alpha - \sigma_{xx}^\alpha + 2i\sigma_{xy}^{(\alpha)} = 2[\bar{z}\phi''_\alpha(z) + \psi''_\alpha(z)], \tag{A3}$$

where $\bar{f}$ is the conjugate of f while f' and f'' indicate the first and the second derivative of the analytic function f, respectively. In our model the phase with $\alpha=1$ corresponds to the matrix and the phase with $\alpha=2$ corresponds to the inclusion. It means that $\phi_1(z)$ and $\psi_1(z)$ are defined for $|z|>R_1$ and $\phi_2(z)$ and $\psi_2(z)$ are defined for $|z|<R_2$. Moreover, the parameter χ_α introduced in Eq. (A1) is given by $\chi_\alpha=3-4\nu_\alpha$ under the assumed plane strain conditions.[28] The solution of the elastic problem can be obtained by imposing the perfect bonding at the interface described by the following continuity relations:

$$(z + u_x^1 + iu_y^1)|_{z=R_1e^{i\theta}} = (z + u_x^2 + iu_y^2)|_{z=R_2e^{i\theta}},$$

$$(\hat{\sigma}^1 \cdot \vec{n})|_{z=R_1e^{i\theta}} = (\hat{\sigma}^2 \cdot \vec{n})|_{z=R_2e^{i\theta}}.$$

These boundary conditions can be expressed in terms of the elastic potentials,

$$\left(z + \frac{1}{2\mu_1}[\chi_1\phi_1 - z\overline{\phi'_1} - \overline{\psi_1}]\right)\Bigg|_{z=R_1e^{i\theta}} = \left(z + \frac{1}{2\mu_2}[\chi_2\phi_2 - z\overline{\phi'_2} - \overline{\psi_2}]\right)\Bigg|_{z=R_2e^{i\theta}}, \tag{A4}$$

$$(\phi_1 + z\overline{\phi'_1} + \overline{\psi_1})|_{z=R_1e^{i\theta}} = (\phi_2 + z\overline{\phi'_2} + \overline{\psi_2})|_{z=R_2e^{i\theta}}. \tag{A5}$$

The potentials $\phi_2(z)$ and $\psi_2(z)$ can be represented by Taylor series and $\phi_1(z)$ and $\psi_1(z)$ by Laurent series.[33,34] A detailed analysis of the problem proves that the following simplified representations are sufficient to solve the problem:

$$\psi_1(z) = \mu_1(\varepsilon_{yy}^\infty - \varepsilon_{xx}^\infty + 2i\varepsilon_{xy}^\infty)z + \frac{H_1}{z} + \frac{H_3}{z^3}, \tag{A6}$$

$$\phi_1(z) = \frac{\mu_1(\varepsilon_{xx}^\infty + \varepsilon_{yy}^\infty)z}{\chi_1 - 1} + \frac{F}{z}, \tag{A7}$$

$$\psi_2(z) = Az, \tag{A8}$$

$$\phi_2(z) = Bz. \tag{A9}$$

The linear terms in $\phi_1(z)$ and $\psi_1(z)$ represent the remotely applied load described by an arbitrary strain with components $\varepsilon^{\infty}_{xx}$, $\varepsilon^{\infty}_{yy}$, and $\varepsilon^{\infty}_{xy}$. The continuity relations given in Eq. (A4) and Eq. (A5) lead to a linear system for the complex parameters H_1, H_3, F, A, and B. The parameters H_1, H_3, and F describe the elastic fields in the matrix around the inclusion and can be eventually obtained as

$$\Re e\{H_1\} = 4\frac{\mu_1\mu_2(R_1 - R_2)R_1^2}{2\mu_2 R_1 - \mu_1 R_2 + R_2\mu_1\chi_2} + 2\frac{(\varepsilon^{\infty}_{xx} + \varepsilon^{\infty}_{yy})[R_1\mu_2(\chi_1 - 1) - R_2\mu_1(\chi_2 - 1)]\mu_1 R_1^2}{(2\mu_2 R_1 - \mu_1 R_2 + R_2\mu_1\chi_2)(\chi_1 - 1)}, \tag{A10}$$

$$\Im m\{H_1\} = 0, \tag{A11}$$

$$\Re e\{H_3\} = \frac{R_1^4\mu_1(\varepsilon^{\infty}_{yy} - \varepsilon^{\infty}_{xx})(\mu_2 R_1 - \mu_1 R_2)}{R_1\mu_2\chi_1 + \mu_1 R_2}, \tag{A12}$$

$$\Im m\{H_3\} = 2\frac{\mu_1 R_1^4\varepsilon^{\infty}_{xy}(\mu_1 R_2 - \mu_2 R_1)}{R_1\mu_2\chi_1 + \mu_1 R_2}, \tag{A13}$$

$$\Re e\{F\} = \frac{R_1^2\mu_1(\varepsilon^{\infty}_{yy} - \varepsilon^{\infty}_{xx})(\mu_2 R_1 - \mu_1 R_2)}{R_1\mu_2\chi_1 + \mu_1 R_2}, \tag{A14}$$

$$\Im m\{F\} = 2\frac{\mu_1 R_1^2\varepsilon^{\infty}_{xy}(\mu_1 R_2 - \mu_2 R_1)}{R_1\mu_2\chi_1 + \mu_1 R_2}. \tag{A15}$$

The parameters A and B represent the uniform field in the cylindrical inclusion

$$\Re e\{A\} = \frac{R_1\mu_1\mu_2(\varepsilon^{\infty}_{yy} - \varepsilon^{\infty}_{xx})(\chi_1 + 1)}{R_1\mu_2\chi_1 + \mu_1 R_2}, \tag{A16}$$

$$\Im m\{A\} = 2\frac{\mu_1\mu_2 R_1\varepsilon^{\infty}_{xy}(\chi_1 + 1)}{R_1\mu_2\chi_1 + \mu_1 R_2}, \tag{A17}$$

$$\Re e\{B\} = 2\frac{\mu_1\mu_2(R_1 - R_2)}{2\mu_2 R_1 - \mu_1 R_2 + R_2\mu_1\chi_2} + \frac{(\varepsilon^{\infty}_{xx} + \varepsilon^{\infty}_{yy})(\chi_1 + 1)R_1\mu_2\mu_1}{(2\mu_2 R_1 - \mu_1 R_2 + R_2\mu_1\chi_2)(\chi_1 - 1)}, \tag{A18}$$

$$\Im m\{B\} = 0. \tag{A19}$$

The knowledge of all the parameters allows us to obtain any component of any elastic field by means of the Kolossov-Muskhelishvili Eqs. (A1)–(A3). It is possible to verify that, if we consider $R_1 = R_2$, we exactly obtain the results of the Eshelby theory for a cylindrical inclusion.[31] Our general solution takes into account both the effects of the remotely applied loads and those induced by the different size between the cylinder and the hosting hole (prestrain). If we suppose to consider the case where no loads are applied to the system, we obtain only two not vanishing parameters, namely, $\Re e\{H_1\}$ and $\Re e\{B\}$. Indeed, in both Eq. (A10) and Eq. (A18) only the first term is independent on the applied loads. Therefore, the parameter $\Re e\{B\}$ describes the uniform isotropic compression inside the cylinder (internal prestrain) while $\Re e\{H_1\}$ describes the asymptotically vanishing (as $1/z$) compression in the matrix (external prestrain). By substituting the expression of $\Re e\{B\}$ (with no loads) in Eq. (A1) we eventually obtain the internal isotropic prestrain ε^0 as

$$\varepsilon^0 = \frac{\mu_1(\chi_2 - 1)(R_1 - R_2)}{2\mu_2 R_1 - \mu_1 R_2 + R_2\mu_1\chi_2}. \tag{A20}$$

This equation has been used in the main text to obtain the fitting of the atomistic prestrain fields through suitable values of the difference $\Delta R = R_2 - R_1$.

*pierluca.palla@dsf.unica.it
†stefano.giordano@dsf.unica.it
‡luciano.colombo@dsf.unica.it

[1] K. Bertoldi, D. Bigoni, and W. J. Drugan, J. Mech. Phys. Solids **55**, 1 (2007).
[2] K. Bertoldi, D. Bigoni, and W. J. Drugan, J. Mech. Phys. Solids **55**, 35 (2007).
[3] V. Holý, G. Springholz, M. Pinczolits, and G. Bauer, Phys. Rev. Lett. **83**, 356 (1999).
[4] M. Schmidbauer, Sh. Seydmohamadi, D. Grigoriev, Zh. M. Wang, Yu. I. Mazur, P. Schäfer, M. Hanke, R. Köhler, and G. J. Salamo, Phys. Rev. Lett. **96**, 066108 (2006).
[5] P. Sharma and S. Ganti, Phys. Status Solidi B **234**, R10 (2002).
[6] M. Yang, J. C. Sturm, and J. Prevost, Phys. Rev. B **56**, 1973 (1997).
[7] X. Zhang and P. Sharma, Phys. Rev. B **72**, 195345 (2005).
[8] J. Singh, *Physics of Semiconductors and Their Heterostructures* (McGraw-Hill Higher Education, New York, 1992).
[9] R. Maranganti and P. Sharma, in *Handbook of Theoretical and Computational Nanotechnology*, edited by M. Reith and W. Schommers (American Scientific Publishers, California, 2006).
[10] R. Timm, H. Eisele, A. Lenz, L. Ivanova, G. Balakrishnan, D. L. Huffaker, and M. Dahne, Phys. Rev. Lett. **101**, 256101 (2008).
[11] P. Harrison, *Quantum Wells, Wires and Dots: Theoretical and Computational Physics of Semiconductor Nanostructures* (John Wiley and Sons Ltd, Chichester, 2005).
[12] P. Sharma and S. Ganti, J. Appl. Mech. **71**, 663 (2004).
[13] P. Sharma, S. Ganti, and N. Bhate, Appl. Phys. Lett. **82**, 535 (2003).
[14] V. Kumar, *Nanosilicon* (Elsevier, Amsterdam, 2007).
[15] S. Cuenot, C. Fretigny, S. Demoustier-Champagne, and B. Nysten, Phys. Rev. B **69**, 165410 (2004).

[16] T. Namazu, Y. Isono, and T. Tanaka, J. Microelectromech. Syst. **9**, 450 (2000).
[17] H. Sadeghian, C. K. Yang, J. F. L. Goosen, E. van der Drift, A. Bossche, P. J. French, and F. van Keulen, Appl. Phys. Lett. **94**, 221903 (2009).
[18] A. Mattoni and L. Colombo, Phys. Rev. B **78**, 075408 (2008).
[19] A. Mattoni and L. Colombo, Phys. Rev. Lett. **99**, 205501 (2007).
[20] S. Pizzini, M. Acciarri, S. Binetti, D. Cavalcoli, A. Cavallini, D. Chrastina, L. Colombo, E. Grilli, G. Isella, M. Lancin, A. Le Donne, A. Mattoni, K. Peter, B. Pichaud, E. Poliani, M. Rossi, S. Sanguinetti, M. Texier, and H. von Knel, Mater. Sci. Eng., B **134**, 118 (2006).
[21] J. Tersoff, Phys. Rev. B **37**, 6991 (1988).
[22] F. Cleri, P. Keblinski, L. Colombo, S. R. Phillpot, and D. Wolf, Phys. Rev. B **57**, 6247 (1998).
[23] F. Cleri, P. Keblinski, L. Colombo, D. Wolf, and S. R. Phillpot, Europhys. Lett. **46**, 671 (1999).
[24] J. D. Eshelby, Proc. R. Soc. London, Ser. A **241**, 376 (1957).
[25] J. D. Eshelby, Proc. R. Soc. London, Ser. A **252**, 561 (1959).
[26] G. Kolosoff, Ph.D. thesis, Dorpat University, 1909.
[27] G. Kolosoff, Z. Angew. Math. Phys. **62**, 384 (1914).
[28] N. I. Muskhelishvili, *Some Basic Problems in the Mathematical Theory of Elasticity* (Noordhoff, Groningen, 1953).
[29] M. Talamali, V. Petaja, D. Vandembroucq, and S. Roux, Phys. Rev. E **78**, 016109 (2008).
[30] J. Mathiesen, I. Procaccia, and I. Regev, Phys. Rev. E **77**, 026606 (2008).
[31] T. Mura, *Micromechanics of Defects in Solids* (Kluwer Academic, Dordrecht, 1987).
[32] H. C. Yang and Y. T. Chou, J. Appl. Mech. **98**, 424 (1976).
[33] A. E. Green and W. Zerna, *Theoretical Elasticity* (Oxford University Press, Oxford, 1954).
[34] R. J. Atkin and N. Fox, *An Introduction to the Theory of Elasticity* (Dover, New York, 2005).